Engineering Notes

ENGINEERING NOTES are short manuscripts describing new developments or important results of a preliminary nature. These Notes cannot exceed 6 manuscript pages and 3 figures; a page of text may be substituted for a figure and vice versa. After informal review by the editors, they may be published within a few months of the date of receipt. Style requirements are the same as for regular contributions (see inside back cover).

Study of Vortex Breakdown of F-106B by Euler Code

Jenn Louh Pao*
Vigyan Research Associates, Hampton, Virginia

Nomenclature

b	= wing span, ft
C_P	= pressure coefficient
M_∞	= freestream Mach number
P_T	= local total pressure, psf
P_{T_∞}	= freestream total pressure, psf
u	= local axial velocity, fps
V_∞	= freestream velocity, fps
y	= spanwise location, ft
α	= angle of attack, deg

Introduction

OTHER researchers have investigated the numerical results of Euler codes with respect to vortex breakdown of a shed leading-edge vortex system.[1-3] The configurations studied range from simple geometries, such as arrow and cranked-delta wings, to a wing-canard-body configuration. This Note builds on the previous work by applying a Three-Dimensional Euler Aerodynamic Method[4] (TEAM) to a more complex geometry, F-106B, at subsonic speed in order to examine the relationship between off- and on-surface flow features at angles of attack sufficiently large for vortex breakdown to occur. In particular, an examination is made of available flow features to determine those which provide both the necessary and sufficient conditions for vortex breakdown.

Criteria of Vortex Breakdown

Based on converged Euler solutions,[5] the flow structure of the F-106B shed vortex system can be analyzed by examining six flowfield features (see Fig. 1). These include contours of suction pressure and total pressure on the leeward surface together with the contours of axial velocity, total pressure, spanwise upper surface pressure, and velocity vectors at the selected computational crossflow planes.

Vortex breakdown over the wing is postulated to occur with the onset of a negative axial velocity region. This indicates the presence of a reversed flow region. The total pressure region shows there to be a corresponding large area of constant pressure implying the vortex expansion around a stagnant core. In the present analysis, two definitions are used: the reversed flow region is defined as the area where $u/V_\infty \leq 0$, and the total pressure loss region is defined as the area where $P_T/P_{T_\infty} \leq 1$.

Received July 10, 1989; revision received Aug. 1, 1989.

*Research Engineer. Member AIAA.

Numerical Results and Discussions

The F-106B is basically a 60-deg delta wing, which is highly cambered near the rounded leading edge. Figure 2 shows the wing planform and all of its computational crossflow plane locations. The numerical features of the TEAM code are detailed in Ref. 6. The basic criteria used to establish a converged Euler solution required the average residual (root mean square value of the net mass flux) $\leq 10^{-4}$ and the total number of supersonic points in the entire flowfield to differ by <3 between consecutive computation cycles. In general, numerical convergence can be expected, and the converged solutions were obtained within 400 computation cycles using 80,625 node points.

At $M_\infty = 0.4$, the computed results are for α ranging from 19 to 30 deg. Solutions for axial velocity and total pressure, suction pressure, and spanwise upper surface pressure are presented in Figs. 3, 4, and 5, respectively. Figure 3 presents the contours of axial velocity and total pressure at three values of α and is used to show the initiation of reversed flow and vortex core expansion at crossplane 6. At $\alpha = 19$ deg, the primary vortical flow is well developed near the leading edge, and no reversed flow occurs over the wing. When α is increased to 23 deg, a small region of reversed flow is found to occur at crossplane 6 but not at crossplane 5, which implies the initial determination of vortex bursting is between these planes. When α increases from 23 to 26 deg, and then to 28 deg, an examina-

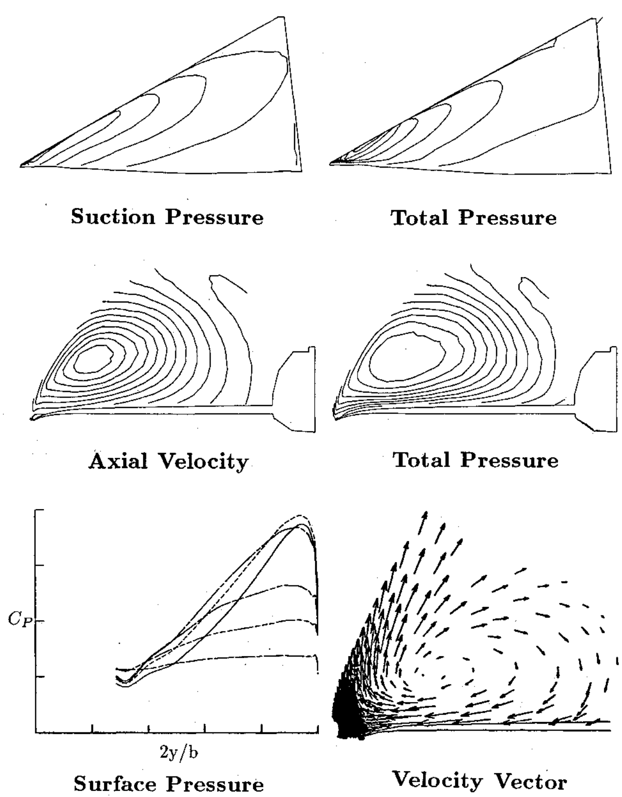

Fig. 1 Six flowfield features examining vortex breakdown phenomenon.

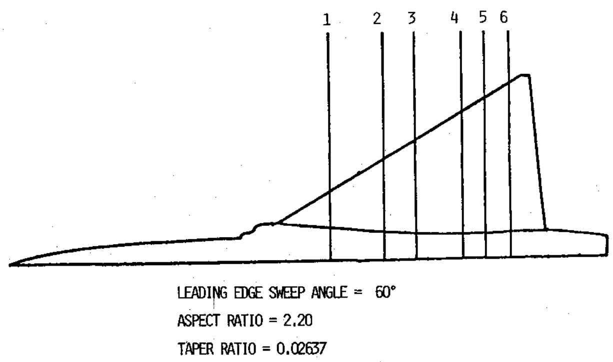

Fig. 2 Longitudinal stations of F-106B crossflow planes.

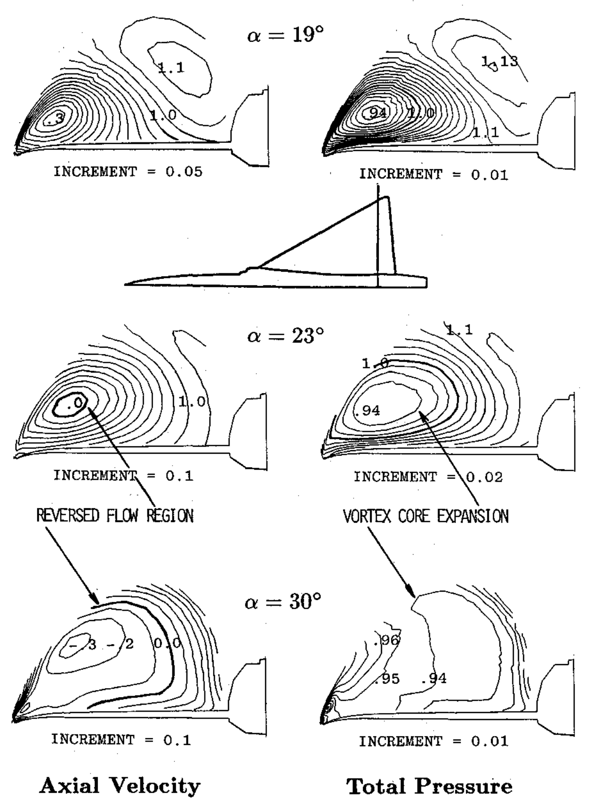

Fig. 3 Effect of α on u/V_∞ contours at crossplane 6 and $M_\infty = 0.4$.

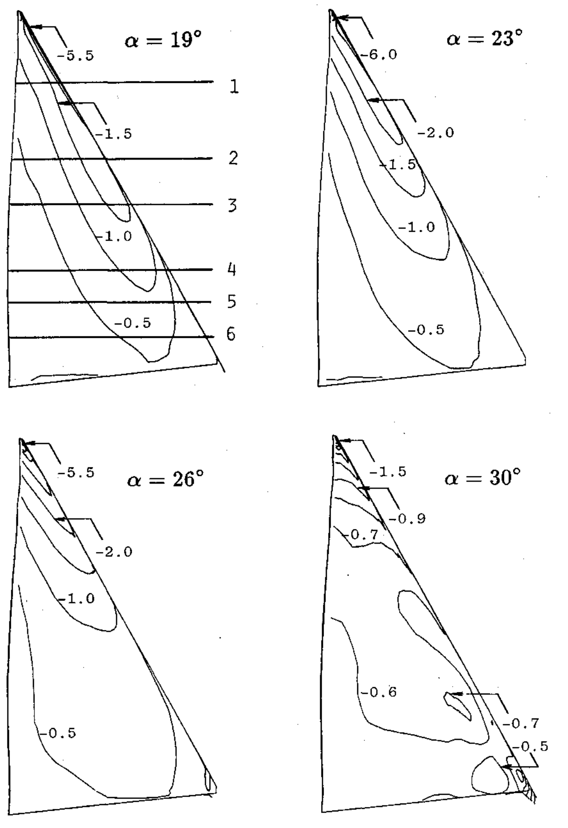

Fig. 4 Effect of α on leeward surface C_P contours at $M_\infty = 0.4$.

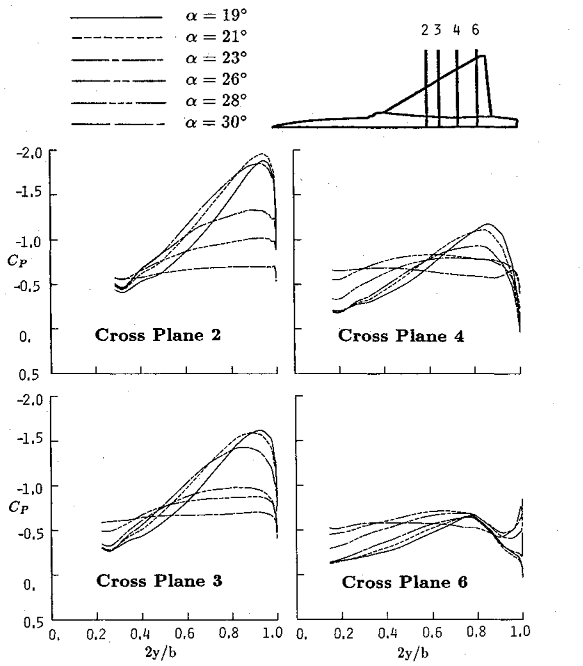

Fig. 5 Effect of α on the spanwise upper surface C_P at four longitudinal stations and $M_\infty = 0.4$.

tion of the axial velocity data shows that the reversed flow region extends as far forward as crossplanes 4 and 2, respectively.

Figures 3–5 are used together to aid in understanding the vortex response with increasing α. The contours of suction pressure in Fig. 4 show the effect of α on the vortex interaction with the wing leeward surface. The corresponding spanwise upper surface pressure distributions at six angles of attack are compared in Fig. 5 for crossplanes 2–4 and 6. First, it is noted from Fig. 3 that as α increases from 19 deg, the size of the vortex core region initially expands, and the center of the region moves upward and inboard, typified by the 19- and 23-deg results. Thus, the combination of these two vortex features (core size and movement) can lead to a reduction in the peak suction value and a spreading out of the associated pressure as shown in Fig. 5. This peak suction value monotonically decreases toward the trailing edge due to the three-dimensional trailing-edge effect. Second, even though the results in Fig. 4 denote the presence of organized vortical flow at $\alpha = 23$ and 26 deg over the entire wing, nevertheless, these results contradict those of Figs. 3 and 5 at crossplane 6. There Fig. 3 indicates an increasing large region of reversed flow for $\alpha \geq 23$ deg, and Fig. 5 indicates an unusual flow behavior (be it attached or unreal) commencing near the leading edge. Therefore, from Fig. 4, it is learned that sharply defined leeward surface pressure contours are a necessary condition for vortex stability but not a sufficient one, whereas the flow features from Fig. 3 can provide both the necessary and sufficient conditions for vortex stability and breakdown.

By contrast, for $\alpha = 30$ deg, the solution did not converge even in 1000 computation cycles and cannot therefore be directly compared with the others. However, an examination of the results developed at the 1000th cycle is a useful exercise. For example, Fig. 4 shows the vortex interaction become totally disorganized on the leeward surface, and a significant drop of the spanwise upper surface pressure is noted in Fig. 5. These figures imply that the vortex breakdown effect becomes dominant over the entire wing. The flowfield unsteadiness was noted in that the crossflow patterns at each computation stage continued to change throughout the solution process; that is, a nonstationary flowfield was observed.

To validate the numerical simulation of vortex breakdown phenomenon by the TEAM code, the experimental results of a 60-deg, sharp-edge, uncambered delta wing by Wentz and Kohlman[7] were qualitatively compared. Their data showed the initiation of vortex breakdown to occur at the trailing edge by $\alpha = 15$ deg; the maximum lift by $\alpha = 30$ deg; and breakdown point moved into apex region by $\alpha = 32$ deg, consequently causing a decrease in lift. By comparison, for this cambered 60-deg delta wing, the TEAM code yields converged results even with a large region of reversed flow over the wing as α increases from 23 to 28 deg. Although the corresponding peak suction value at the examined crossflow planes are shown to be more positive, nevertheless, due to a larger vortex interaction with the leeward surface (see Fig. 5), the total lift continues to increase. In Ref. 5, the computed lift characteristics in this α range compare reasonably well with the experimental data for the F-106B configuration. As the region of reversed flow moves into the apex region by $\alpha = 30$ deg, the solution does not converge.

Summary

The three-dimensional vortex breakdown phenomenon over a F-106B configuration has been studied by examining a variety of on- and off-surface flow features from the TEAM code. Although the flow separation of this code is triggered by the numerical dissipation, and the computed flowfield may not represent the real vortex breakdown phenomenon adequately, nonetheless, the general trend of vortex breakdown effect on computed lift characteristics is similar to the wind tunnel results. Of the flowfield features examined, the crossflow contours of axial velocity and total pressure can provide both the necessary and sufficient conditions for vortex stability and breakdown.

Acknowledgment

This research work was supported by NASA Langley Research Center under Contract NAS1-17919, with John E. Lamar as the technical monitor.

References

[1]Hitzel, S. M. and Schmidt, W., "Slender Wings with Leading Edge Vortex Separation—A Challenge for Panel Methods and Euler Solvers," *Journal of Aircraft*, Vol. 21, Oct. 1984, pp. 751–759.

[2]Rizzi, A. and Purcell, C. J., "Disordered Vortex Flow Computed Around a Cranked Delta Wing and at Subsonic Speed and High Incidence," International Council of Aeronautical Sciences, Paper ICAS-86-1.4.1, Sept. 1986.

[3]Raj, P., Keen, J. M., and Singer, S. W., "Applications of an Euler Aerodynamic Method to Free-Vortex Flow Simulation," *Proceedings of the AIAA 6th Applied Aerodynamics Conference*, AIAA, New York, June 1988.

[4]Raj, P. and Brennan, J. "Improvements to an Euler Aerodynamic Method for Transonic Flow Analysis," AIAA Paper 87-0040, Jan. 1987.

[5]Pao, J. L., "Vortex Flow Analysis for F-106B Configuration," *Proceedings of the First National Fluid Dynamics Congress*, AIAA, Washington, DC, July 1988.

[6]Agarwal, R. K. and Deese, J. E. "Transonic Wing-Body Calculations Using Euler Equations," AIAA Paper 83-0501, Jan. 1983.

[7]Wentz, W. H. and Kohlman, D. L., "Vortex Breakdown On Slender Sharp-Edge Wings," AIAA Paper 69-778, July 1969.

Incompressible Viscous Flow About Aircraft Configurations

K. P. Sinhamahapatra,* N. Singh,† and B. C. Basu‡
Indian Institute of Technology, Kaharagpur, India

Nomenclature

A_{ik}, B_{ik}, C_{ik}, D_{ik}	= normal components of velocities induced at the jth collocation point by the kth surface source, bound vorticity, line source, and horseshoe vortex respectively
$Æ$	= aspect ratio
C_L	= total lift coefficient
C_l	= sectional lift coefficient
$C_{M_{LE}}$	= pitching-moment coefficient about wing leading edge
C_P	= pressure coefficient
c	= chord, m
D	= fuselage diameter (Fig. 2), m
h_1, h_2, g	= metrics of the nonorthogonal curvilinear coordinate system used in three-dimensional boundary-layer calculation
L_0	= fuselage length, m
N_T	= total number of singularities
$\hat{n}$	= outward unit normal vector
q	= function of metrics, ($q^2 = h_1^2 h_2^2 - g^2$)
R_N	= Reynolds number
s	= semispan, m
u_e	= resultant velocity at the edge of boundary layer
V	= total velocity vector
V_{ik}	= generalized induced velocity at the jth control point due to the kth generalized singularity
V_∞	= freestream velocity vector
W_{iw}	= transpiration velocity
α	= angle of attack
Γ	= strength of horseshoe vortex
γ	= vorticity strength
Δ_1, Δ_2	= displacement thicknesses in the nonorthogonal curvilinear coordinate system
δ_1, δ_2	= streamwise and cross-flow displacement thicknesses
ϵ	= wing setting angle
Π_k	= generalized singularity
σ	= source strength
Ω_{LE}	= leading-edge sweep back

Subscripts

t	= tail quantity
w	= wing quantiy

Received June 22, 1989; revision received July 31, 1989.

*Research Staff, Aeronautical Engineering Department.
†Assistant Professor, Aeronautical Engineering Department.
‡Professor, Aeronautical Engineering Department.